LUND UNIVERSITY

Hyperfine-structure investigation of highly excited ^(2)D levels in Rb 87 and Cs 133 using a cw tunable dye laser in a two-step excitation scheme

Svanberg, Sune; Tsekeris, P

Published in:
Physical Review A (Atomic, Molecular and Optical Physics)

DOI:
10.1103/PhysRevA.11.1125

1975

Link to publication

Citation for published version (APA):
Svanberg, S., & Tsekeris, P. (1975). Hyperfine-structure investigation of highly excited ^(2)D levels in Rb 87 and Cs 133 using a cw tunable dye laser in a two-step excitation scheme. *Physical Review A (Atomic, Molecular and Optical Physics)*, *11*(4), 1125-1137. https://doi.org/10.1103/PhysRevA.11.1125

Total number of authors:
2

General rights
Unless other specific re-use rights are stated the following general rights apply:
Copyright and moral rights for the publications made accessible in the public portal are retained by the authors and/or other copyright owners and it is a condition of accessing publications that users recognise and abide by the legal requirements associated with these rights.
• Users may download and print one copy of any publication from the public portal for the purpose of private study or research.
• You may not further distribute the material or use it for any profit-making activity or commercial gain
• You may freely distribute the URL identifying the publication in the public portal

Read more about Creative commons licenses: https://creativecommons.org/licenses/

Take down policy
If you believe that this document breaches copyright please contact us providing details, and we will remove access to the work immediately and investigate your claim.

LUND UNIVERSITY

PO Box 117
221 00 Lund
+46 46-222 00 00

Hyperfine-structure investigation of highly excited ^2D levels in ^{87}Rb and ^{133}Cs using a cw tunable dye laser in a two-step excitation scheme*

S. Svanberg[†‡] and P. Tsekeris

Columbia Radiation Laboratory, Department of Physics, Columbia University, New York, New York 10027

(Received 12 December 1974)

The hyperfine structure of several highly excited ^2D states in ^{87}Rb and ^{133}Cs has been measured. The D-state atoms were produced in a two-step–excitation process. In the first step, multiple scattering of the strong alkali-metal D_1 and D_2 lines from an rf lamp was used to excite atoms into the first excited ^2P levels. The intense tunable radiation from a cw dye laser was used in the second step to transfer P-state atoms into highly excited D states. Level-crossing and optical-double-resonance techniques were used for the determination of the absolute values of the hyperfine-interaction constants. The following results (in MHz) were obtained for the magnetic dipole and the electric quadrupole interaction constants a and b: For ^{87}Rb, $|a(6\,^2D_{3/2})| = 7.84(5)$, $|b(6\,^2D_{3/2})| = 0.53(6)$ $(b/a > 0)$, $|a(6\,^2D_{5/2})| = 3.6(7)$, $|a(7\,^2D_{3/2})| = 4.53(3)$, $|b(7\,^2D_{3/2})| = 0.26(4)$ $(b/a > 0)$, $|a(7\,^2D_{5/2})| = 2.2(5)$. For ^{133}Cs, $|a(8\,^2D_{3/2})| = 3.98(8)$, $|a(8\,^2D_{5/2})| = 0.9(4)$, $|a(9\,^2D_{3/2})| = 2.37(3)$, $|a(9\,^2D_{5/2})| = 0.5(2)$, $|a(10\,^2D_{3/2})| = 1.52(3)$, $|a(10\,^2D_{5/2})| = 0.4(2)$. The a factors generally deviate strongly from the values expected in a one-electron picture of the alkali-metal atom indicating the importance of polarization and correlation effects for these states. For ^{87}Rb a comparison with a recent calculation including polarization effects is made. The b factors for ^{87}Rb are the first significant values allowing a calculation of an alkali-metal-atom nuclear quadrupole moment from non-P-state data.

I. INTRODUCTION

The alkali-metal atoms have a particularly simple electronic structure and a very detailed theoretical understanding of their properties could perhaps be expected. An atom with a single electron moving in the combined potential from the nucleus and a core of closed electron shells is certainly well understood and an accurate diagram of electronic energy levels can be constructed without too much effort. The spin dependence of the exchange forces between the valence electron and the individual core electrons can, however, give rise to an imbalance (polarization) in the closed electron shells, which can be interpreted in terms of excitation of core electrons to outer orbits. Whereas such core excitations have a minor effect on the gross features in the energy-level diagram, such atomic parameters as fine- and hyperfine-structure coupling constants can be appreciably affected. The breakdown of a pure one-electron description of the alkali atom is evident from a study of the fine-structure intervals for D and F doublets.[1] Many of these doublets are anomalously narrow or even inverted.

Investigations of the hyperfine structure (hfs) of excited states in alkali atoms are of great interest not only from the point of view of an understanding of the basic atomic interactions, but also for the determination of nuclear moments.[2] The investigations require high-resolution methods like optical double resonance (ODR) or level crossing (LC) as the hfs is generally small compared to the Doppler width of the optical lines. Until recently accurate experimental studies of alkali-metal hfs have been confined to the sequences of P states, which are readily available for observation through direct excitation with resonance radiation.

So far D-state hfs data has been very limited. Studies of non-P states have been obstructed by the difficulty to produce such states. Archambault *et al.*[3] could circumvent the selection rules for electric dipole radiation by using electron bombardment and could make rough estimates of the hfs of the $5\,^2D_{5/2}$ state in Na^{23} and the $9\,^2D_{5/2}$ state in Cs^{133}. With the recently introduced cascade decoupling[4] and cascade rf spectroscopy methods[5] the Columbia group has investigated the hfs of several low-lying S and D levels in the alkali-metal atoms.[6]

Recently we have reported a two-step excitation method which allows us to get access to more highly excited states in the alkali atoms.[7] In the first step the strong D_1 and D_2 lines from an rf lamp are used to transfer atoms from the ground S state to the first excited P states. In the second step the intense, tunable radiation from a cw dye laser, operating with rhodamine 6G, is used to excite atoms from one of the P levels to a highly excited S or D level. From such levels, P and F levels are also populated in the cascade decay. Using this method in conjunction with conventional ODR and LC techniques we have reported preliminary results for the absolute values of the hyperfine coupling constants for a number of highly excited D and F levels in Rb and Cs.[8] We have now

Copyright © 1975 by The American Physical Society.

extended our measurements to other states and increased the accuracy, and the results for ten D states in ^{87}Rb and ^{133}Cs are reported in this work.

In Sec. II of this paper the two-step excitation method is described. In Sec. III some brief theoretical comments on the various experiments are made. Experimental details are given in Sec. IV. In Sec. V we describe our ODR and LC measurements. Finally, the results are analyzed in Sec. VI.

II. TWO-STEP OPTICAL EXCITATION IN CONJUNCTION WITH A DYE LASER LIGHT SOURCE

As electric dipole transitions connect states of opposite parity, a two-step process is needed for a radiative transfer of atoms between states of the same parity. A cascade method[4] or a two-step excitation scheme has to be used. The process of two successive optical excitations is in general not very probable because of the short lifetime of the intermediate atomic state. The success of a two-step excitation experiment thus very much relies on the efficiency of the light sources.[9-11] With the great achievements in the technology of tunable lasers, very efficient light sources have become available for atomic spectroscopy.[12-14]

The principles of the two-step excitation method that we have used are shown in Figs. 1 and 2, where the explicit case of cesium has been chosen. Figure 1 displays the cesium level diagram with the D_1 and D_2 lines, used in the first excitation step, indicated. These lines are produced by a powerful rf lamp. The cw operation region for the tunable laser, using rhodamine 6G as a dye, is indicated on the wavelength scale, starting from the first excited ^2P levels. Thus the most convenient wavelength region for a cw dye laser in the second excitation step covers a large number of levels just above those levels which can still be investigated by cascade rf spectroscopy using a single conventional lamp.[5] In Fig. 2 the scattering-cell arrangement and the observation of light released after a two-step excitation of the $9\,^2D_{5/2}$ Cs level is illustrated. Here the laser was tuned to the $6\,^2P_{3/2}$-$9\,^2D_{5/2}$ transition. The light was observed in the second step of the two-step decay, as the light emitted in the first step ($9\,^2D_{5/2}$-$7\,^2P_{3/2}$) consists of ir photons, which cannot be detected by ordinary photomultiplier tubes. The two light sources are at right angles to each other and the volume in the resonance cell where atoms interact with both light beams is about 0.5 cm^3. In the detection beam a filter is inserted, which selects the detection line and suppresses the laser and the lamp lines as much as possible. However, a direct leakage of the detection line from the rf-lamp line spectrum can of course only be prevented by a filter, eliminating this line from the rf-lamp output. From the recording in the right part of Fig. 2 it is seen that with the filters we used in this particular case there is no direct leakage of lamp light, whereas a substantial laser-light leakage into the detection channel is evident. With proper filters, however, unwanted light can be completely suppressed. With the laser we have used it was possible to sit on a line without retuning for $\frac{1}{2}$ to 1 h. We did not use any temperature stabilization of our laser environment.

In a two-step excitation process it is essential to produce a reasonably large population of atoms in the intermediate level. As the lifetime of the first ^2P states in the alkali metals is only a few tens of nanoseconds (30 nsec for Cs) a high pumping rate is needed. This is of course most efficiently accomplished with a tunable laser in this step too. However, cw tunable dye lasers so far do not operate at the wavelengths proper for the heaviest alkali atoms. It is instead possible to work with an rf lamp and take advantage of radiation trapping of the D_1 and D_2 lines, which have an absorption oscillator strength close to unity. At a high atomic density, in the multiple-scattering process, an incoming photon can excite several ground-state atoms into a ^2P state[11] so that more P-state atoms will be available for laser excitation. Thus at the usual operating temperatures (~100 °C for Cs, ~120 °C for Rb) with about 10^{13} ground-state atoms per cm^3 we estimate that we have ~10^9 P-state atoms in the interaction volume assuming 10^3 primary excitations per atom per second and ten steps in a multiple-scattering chain. Experimentally we detect 10^6–10^8 photons/sec in a solid angle of about 0.15 sr, depending on what particular state is studied and what detection line is used. Considering also branching ratios and the quantum efficiency of the photomultiplier cathode we conclude that we have in total 10^{10}–10^{12} laser excitations per second out of the ^2P state. Because of the mode structure of the dye laser (mode spacing 550 MHz, mode width ~50 MHz) only about $\frac{1}{10}$ of the ^2P-state atoms, which have Doppler distributions of half-widths close to 1000 MHz, have the right velocity with respect to the laser-beam direction to be excited by the laser. In multimode operation our laser has about 50 competing modes between which we have a very rapid mode hopping. Thus, a large fraction of the total time the laser is lasing on modes which do not "hit" the desired atomic transition. However, due to the quick mode hopping we still have a quasicontinuous excitation. Regarding the above facts we conclude

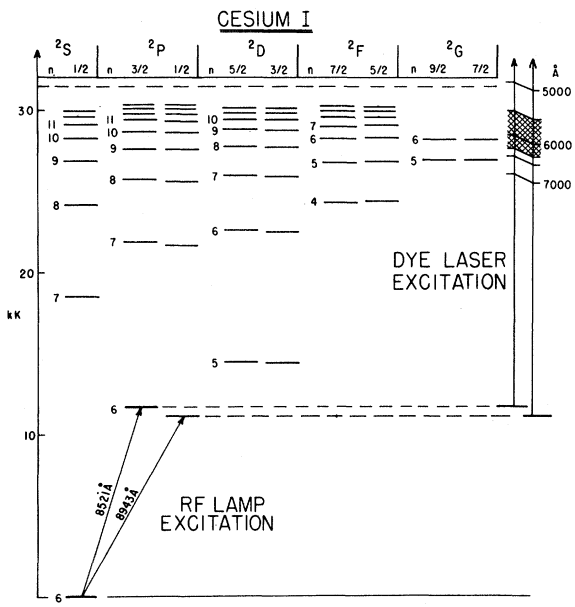

FIG. 1. Energy-level diagram for Cs, with wavelengths relevant for two-step excitation indicated.

that at times when the laser hits the atoms we have an excitation rate of the order of 10^3–10^5 per second for the atoms in the right velocity groups. Typical decay rates for the highly excited states investigated in this work are ~10^7 per second. Thus, light-induced broadening and light shifts in the resonances we observe should be negligible. Experimentally this is also verified. In testing experiments, where different light intensities were used we see no significant influence on well-resolved signals.

The excitation scheme we have employed can conveniently be used in conjunction with conventional ODR and LC techniques with continuous photon detection. As the mode-hopping frequency is sufficiently high the light-intensity fluctuations can be averaged out using a reasonably small time constant on the lock-in amplifier. Of course the signal-to-noise ratio is much improved if single-mode operation is used. With a pulsed dye laser pumped by a flash-lamp or a nitrogen laser, high peak powers are easily obtained and saturation is reached for the transitions. However the low duty cycle of such systems (typically 1 part in 10^5) causes an average counting rate much inferior to what is obtained with a low-power cw laser. In addition, the strong peak powers at pulsed lasers cause shifts and broadening of resonance lines so that a continuous photon detection in ODR and LC experiments cannot be used even if a high repetition rate is employed. Pulsed lasers are thus less suitable for the type of experiments we have performed.

III. THEORETICAL COMMENTS ON hfs DETERMINATIONS

The hfs of an atomic energy level in the presence of a homogeneous external magnetic field H is adequately described by the Hamiltonian[2]

$$H = ah\vec{I}\cdot\vec{J} + bh\frac{3(\vec{I}\cdot\vec{J})^2 + \frac{3}{2}\vec{I}\cdot\vec{J} - I(I+1)J(J+1)}{2I(2I-1)J(2J-1)} + g_J\mu_B H J_z - g_I'\mu_B H I_z \ . \quad (1)$$

Here the first term describes the magnetic dipole interaction between the nucleus of spin angular momentum $\vec{I}$ and the electronic shell with a total angular momentum $\vec{J}$. The dipole interaction constant a gives the characteristic strength of the interaction. Similarly, the second term represents the electric quadrupole interaction between the nucleus and the electronic shell, and the quadrupole interaction constant b gives the strength of the coupling. The third and fourth terms describe the direct interaction between the magnetic field and the electronic and nuclear magnetic moment, respectively. The strength of the coupling is pro-

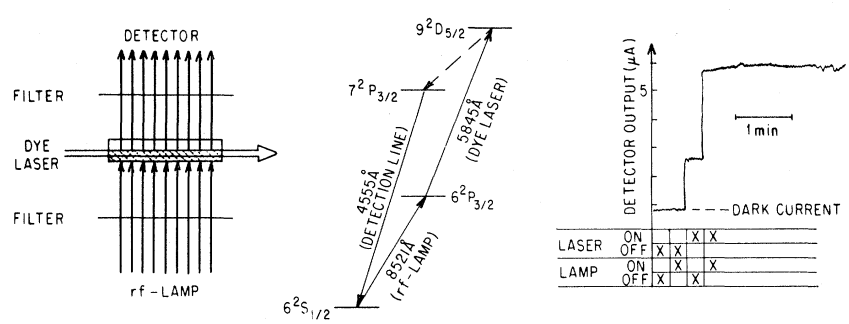

FIG. 2. Left: Scattering-cell arrangement with the different light beams indicated. Center: Energy-level diagram illustrating the two-step excitation of the $9\,^2D_{5/2}$ level in Cs. The fluorescent light is detected in the second step of the two-step decay back to the ground state. Right: Recording of the detector output for the situation shown in the center of this figure. Various excitation combinations are shown to illustrate the two-step excitation process.

portional to the electronic g_J factor and the nuclear g_I' factor, respectively. For a system with one electron outside completely closed shells the Landé g_J factor is given by

$$g_J = (g_s - 1)\frac{j(j+1) - l(l+1) + s(s+1)}{2j(j+1)} + 1 \ . \qquad (2)$$

Here the quantum numbers have their usual meaning, and we have $g_s = 2.002\,32$. The Schwinger correction factor has been applied to g_s. For alkali-metal atom S and P states, Eq. (2) has proved to be valid to a high accuracy (better than 0.2%).[15] For D states, (2) yields $g_J\ (^2D_{3/2}) = 0.7995$ and $g_J\ (^2D_{5/2}) = 1.2005$.

Corresponding to the Hamiltonian (1) the energy-level diagram for the hfs of an electronic level is obtained by diagonalization of the corresponding energy matrix. In Fig. 3 a level diagram for a $^2D_{3/2}$ state in ^{87}Rb is shown as an example. Here dimensionless units have been used for energy and magnetic field. The goal of ODR and LC experiments is to determine the values for, or relations between the characteristic constants a, b, g_J, and g_I by observing energy-level crossovers or rf resonances between magnetic sublevels. We have used the LC method for the study of the hfs of the highly excited $^2D_{3/2}$ states in ^{87}Rb and ^{133}Cs, whereas the ODR method proved to be more useful for the corresponding $^2D_{5/2}$ states.

In Fig. 3 four crossing points between levels with magnetic quantum numbers m differing by 2 units ($\Delta m = 2$ crossings) are indicated. In a resonance scattering experiment, in which a coherent excitation of magnetic sublevels and a likewise coherent detection is made, the high-field level crossings, like the zero-field crossing (Hanle effect), are observed as a change in the intensity and polarization distribution of the fluorescence light. The details of a scattering process involving an initial state i, an excited state e, and a final state f are given by the Breit-Franken formula for the scattered intensity $R(\hat{e}, \hat{u})$[16]:

$$R(\hat{e},\hat{u}) = C_1 \sum_{nn'} \sum_{\mu\nu} \frac{\langle n|\,\hat{e}\cdot\vec{p}\,|\mu\rangle\langle\mu|\,\hat{e}\cdot\vec{p}\,|n'\rangle\langle n'|\,\hat{u}\cdot\vec{p}\,|\nu\rangle\langle\nu|\hat{u}\cdot\vec{p}\,|n\rangle}{\Gamma_e + i\omega_{nn'}} \ . \qquad (3)$$

Here $\hat{e}$ and $\hat{u}$ are the polarization vectors for the exciting and detected light, respectively, and $\vec{p}$ is the momentum operator of the atom. C_1 is a proportionality constant. The summation is made over pairs of magnetic sublevels n and n' in the excited state e and over magnetic sublevels μ and ν in the initial state i and the final state f, respectively. Γ_e is the spontaneous decay rate of the excited state ($\Gamma = 1/\tau$, where τ is the natural lifetime). The energy difference between a pair of excited state sublevels n and n' is $\hbar\omega_{nn'}$. The intra-atomic interference effect leading to the crossing signal takes place only in the region of mutual level overlap within the natural radiative width $\Gamma_e/2\pi = 1/2\pi\tau_e$. In order to obtain a well-resolved signal structure the ratio between the hfs and the radiative width should be appreciable. For $a/(\Gamma/2\pi) \geq 10$ nicely resolved signals are generally obtained. By choosing a proper geometrical arrangement, to be described later, the level-crossing signals can be detected with Lorentzian line shapes in a good resolution case.

From the Hamiltonian (1) and Fig. 3 it is evident that by measuring the positions of the crossings only the ratios a/g_J and b/g_J can be determined. In practice, the g_J-independent ratio b/a is determined from the relative positions of the crossings. With b/a given, the a value is obtained from the actual crossing field values using an experimental g_J factor or by utilizing (2).

Equation (3) is derived under the assumption of equal populations for all the sublevels of the initial state and excitation with light with a "white" frequency distribution. An analysis of level-crossing data using (3) in cases when $a/(\Gamma/2\pi)$ is small

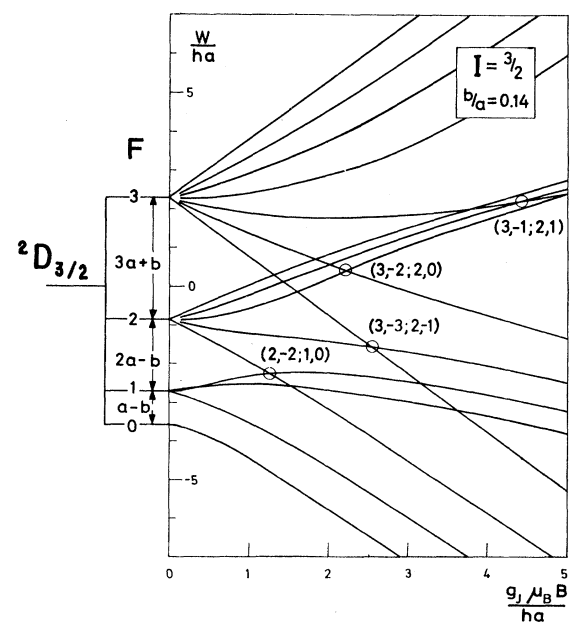

FIG. 3. Energy-level diagram for the hyperfine structure of a $^2D_{3/2}$ level in ^{87}Rb (nuclear spin $I = \frac{3}{2}$). Dimensionless units are used for energy and magnetic field. The $\Delta m = 2$ level crossings are indicated using the symbol $(F, m_F; F', m_F')$, specifying the quantum numbers for the participating levels.

depends critically on the experimental fulfillment of these assumptions. In our case the starting level for the coherent scattering process is a short-lived ^2P state, produced by unpolarized light irradiated in the direction of the magnetic field (σ light). Clearly, the different sublevels get different populations in the primary excitation. In the multiple-scattering process, however, the light has an isotropic nature and the populations level out efficiently. A nonwhite laser excitation is not disturbing as long as individual level-crossing signals can be identified. As unpolarized light in the direction of the magnetic field is used in the first excitation step there is no coherence transfer from the first to the second step.

If the observation of light is not performed directly in the decay of the excited state but in the second step of a two-step decay over a branching state b, the scattering process is described by a formula given by Gupta, Chang, and Happer.[6] Thus

$$R(\hat{e},\hat{u}) = C_2 \sum_{nn'} \sum_{kk'} \sum_{\mu\nu} \langle k|\vec{p}|n\rangle\langle n'|\vec{p}|k'\rangle \times \langle k'|\hat{u}\cdot\vec{p}|\nu\rangle\langle\nu|\hat{u}\cdot\vec{p}|k\rangle \times \langle n|\hat{e}\cdot\vec{p}|\mu\rangle\langle\mu|\hat{e}\cdot\vec{p}|n'\rangle \times (\Gamma_e + i\omega_{nn'})^{-1}(\Gamma_b + i\omega_{kk'})^{-1}\,, \qquad (4)$$

where the summation is over pairs of sublevels n, n' and k, k' in the excited state e and the branch state b, respectively, and over sublevels μ and ν in the initial state i and in the final state f. C_2 is a proportionality constant. The other symbols have the meaning defined in the context of Eq. (3). Equation (4) contains the product of two resonance denominators, one for level crossings in the excited state and one for level crossings in the branch state. Thus it is difficult to observe high field level crossings in cascade experiments unless the crossings in the excited and branch states occur in the same fields within the natural radiative widths. On the other hand the Hanle effect in a cascading process is easily observable.

In ODR experiments rf transitions between differently populated sublevels are detected by a change in the intensity and polarization distribution. ODR experiments are particularly simple to analyze in zero-field-, Zeeman-, or Paschen-Back-region experiments. We performed our ODR experiments in the Paschen-Back region. Using first-order perturbation theory and neglecting the small quadrupole interaction term we obtain for the energy E of a sublevel with quantum numbers m_J and m_I,

$$E = g_J\mu_B H m_J - g_I'\mu_B H m_I + ah m_I m_J\,. \qquad (5)$$

With the selection rules for magnetic dipole transitions $\Delta m_J = \pm 1$, $\Delta m_I = 0$ we obtain, for the Paschen-Back region, rf resonances ν_{m_I},

$$\nu_{m_I} = g_J\mu_B H/h + ahm_I\,. \qquad (6)$$

Thus we obtain $2I+1$ resonances symmetrically spread around the center of gravity corresponding to the particular g_J factor. Like for the LC signals the width of ODR signals are essentially determined by the radiative width of the participating levels. However, a resolved ODR signal broadens with increasing rf amplitude H_1. Thus for the measured full half-width $\Delta\nu$ we have

$$(\Delta\nu)^2 = \frac{1}{\pi^2\tau^2}\left[1 + K(H_1\tau)^2 + \cdots\right]. \qquad (7)$$

Here K is a constant.

The positions of the signals in ODR and LC experiments are the same for normal and inverted hfs. Therefore only the absolute values and the relative signs of a and b can be determined in measurements of the kind we have performed. A number of methods can be used for determining the absolute signs. For example, by observing the signs of dispersion-shaped level-crossing signals a judgement between normal and inverted hfs can be made.[17] The sign of the interaction constants can also be determined by decoupling spectroscopy.[4,6,18] Another method is to perform LC or ODR experiments in parallel magnetic and electric fields. In such experiments the relative signs of the interaction constants a and b and the electronic tensor polarizability α_2 is obtained,[19] and the sign of α_2 can in many cases be calculated with confidence. As a matter of fact the last method has been used for the sign determinations of the states studied in this work. These Stark-effect measurements are described in detail in a different paper.[20]

In performing experiments on the highly excited alkali states it is very valuable to have estimates on absorption oscillator strengths, natural lifetimes, and branching ratios. For the alkali-metal-atom P states the Coulomb approximation method of Bates and Damgaard[21] has proved to be very reliable and an agreement within 10%, between experimental and theoretical lifetimes has generally been obtained. Thus this method should be reliable in predicting the radiative properties of highly excited P and non-P states. We have made extensive computer calculations for the alkali-metal atoms using the Bates and Damgaard method.

IV. EXPERIMENTAL ARRANGEMENT

Our experimental arrangement is based on the apparatus described in Ref. 6. However, a number

of modifications were made and therefore we give a brief description of the setup we have employed. A schematic diagram of our apparatus is shown in Fig. 4.

The generation of light, released after the two-step excitation process, was accomplished in the resonance cell. In most of the experiments we used quartz cells, 15× 20× 65 mm with small flat parallel windows, through which the laser beam passed. The cell was placed in a combined rf cavity and oven. The cells had a stem which could be cooled by compressed air. In this way it became the coolest part of the cell, thus preventing the accumulation of metal on the small windows, which especially in the LC experiments, was intolerable due to the difficulty of adequately eliminating the laser background light with filters. The cells were prepared with a small amount of natural ^{133}Cs or isotopically enriched ^{87}Rb (99.3%).

For the generation of the D_1 and D_2 lines used in the first excitation step, a powerful rf lamp was constructed. An alkali-metal lamp cylinder 80 × 30 mm was placed in an electrically heated oven and was excited in the six-turn coil of a push-pull oscillator. The oscillator operated at about 30 MHz and at a power level of about 150 W. No filling of inert gas was used in the lamp cylinders.

The light for the second excitation step was produced by a tunable dye laser, operating with rhodamine 6G in a methanol solution. We used a Spectra-Physics model 370 dye laser, which was pumped by the 5145-Å line or the all line output of a Spectra-Physics model 165-03 argon-ion laser. The dye laser covered the wavelength region 5550–6300 Å. In multimode operation an output of up to 300 mW is obtained at the peak of the fluorescence curve of rhodamine 6G (~5900 Å), when 2 W in the 5145-Å line of the argon-ion laser is used for the pumping. We calibrated the wavelength scale of the laser by observing with the eye the fluorescence in the D_1 and D_2 lines of a heated Na cell. In the measurements we also frequently used a well-calibrated grating monochromator to set the laser within 1 or 2 Å from the wanted line. The fine tuning was always done by observing the fluorescence light released after the two-step excitation. The dye laser had an output band width of about 0.3 Å (~25 GHz). The output consists of several modes as discussed before. The mode spacing corresponding to a cavity length of 28 cm is ~550 MHz. With an intracavity etalon assembly, consisting of an uncoated 3-mm quartz disk and a 1-mm microscope slide, which could be tilted independently, operation in a few or even a single mode could be achieved with a substantial loss of output power. The studies of the mode structure were made with a piezoelectrically scanned Fabry-Perot interferometer. Several of our measurements were performed with a narrow-band operation.

The output of the dye laser is vertically polarized. To be able to vary the polarization of the laser with respect to the magnetic field direction, thus allowing for π or σ transitions, we used a broad-band polarization rotator. The laser beam had a diameter of about 3 mm as it traversed the resonance cell and the beam was finally dumped on a beam stopper or power meter head. In the figure an alternative laser-beam route is shown. This route was used in measurements where circularly polarized light was employed. A small "Cassegrain" mirror was used to direct the laser beam in the center of the converging rf-lamp beam without obstructing the first-step excitation light

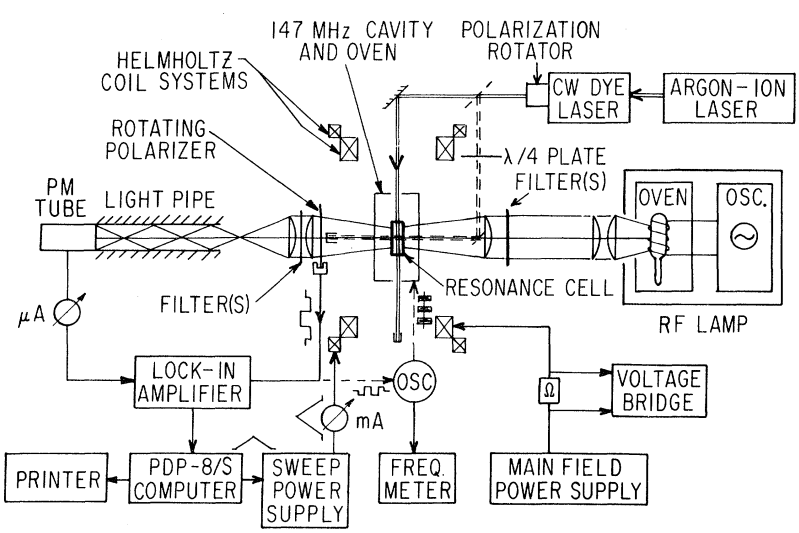

FIG. 4. Experimental arrangement in the two-step excitation experiments. The setup for level-crossing measurements is shown in solid lines, whereas the modifications shown in dashed lines were made for some of the optical-double-resonance measurements.

appreciably. In the rf-lamp beam and the detected beam we used various interference and color glass filters for selecting the detection line and suppressing background light due to the two light sources. In the rf-lamp beam it was generally sufficient to use a Schott RG10 color glass filter which passes more than 90% of the Rb and Cs D_1 and D_2 lines but blocks all non-ir lines. In the detection beam we generally used a 2 in.×2 in. interference filter with a 50-Å bandpass together with a Schott color glass filter to further reduce the unwanted light. The fluorescent light was detected by an RCA C31000 F photomultiplier tube which could be placed away from the region of strong magnetic fields by using a light pipe.

In our measurements we used lock-in techniques for obtaining a good signal-to-noise ratio. In the LC measurements a rotating linear polarizer was used in the detection beam to provide the modulation. A reference signal was taken out from the rotating polarizer and fed to the lock-in amplifier. In the ODR measurements we modulated the rf oscillator with a square wave of low frequency and thus detected the change in the fluorescent light due to the rf transitions. The lock-in signal was stored in a PDP-8/S computer, which also controlled a linear magnetic field sweep. The accumulated signal could be displayed on an oscilloscope and read out on a teletype.

The magnetic field necessary in these measurements was produced in two systems of Helmholtz coils. One system provided a steady field proportional to the voltage reading of a voltage bridge connected over a precision resistor. The other system was used for sweeping the field through the studied signals repetitively in the signal averaging process. The Helmholtz coil systems were

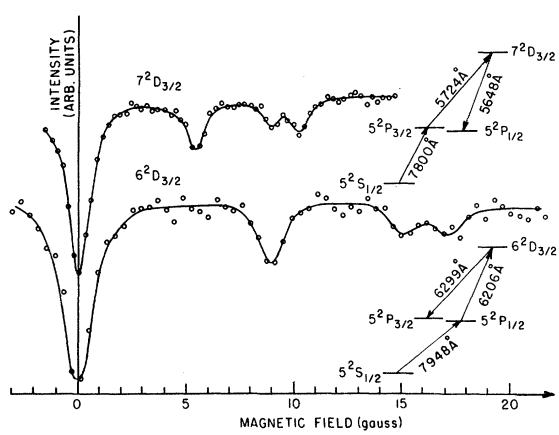

FIG. 5. Level-crossing signals for the 6 and $7\,^2D_{3/2}$ states in ^{87}Rb. The sampling time for each of the curves is about 1.5 h. The solid lines were drawn for the guidance of the eye and are not theoretical fits.

calibrated by optical pumping in ^{85}Rb on several occasions during the run of these experiments. Very consistent results were obtained. For low fields (< 20 G) the main field calibration was accurate to 0.2% and for high fields it was considerably better. The nonlinearity of our sweep field was below 1%. The components of Earth's magnetic field perpendicular to the main field direction were compensated by two additional Helmholtz-coil systems.

For the ODR measurements a 147-MHz cavity was used. The cavity was fed by a General Radio unit oscillator followed by an rf amplification system. The frequency was measured by a digital frequency meter.

V. LEVEL CROSSING AND OPTICAL DOUBLE-RESONANCE MEASUREMENTS

A. Level-crossing measurements on the 6 and 7 $^2D_{3/2}$ levels in ^{87}Rb

The LC method was chosen for measuring the hyperfine coupling constants a and b for the 6 and $7\,^2D_{3/2}$ states in ^{87}Rb. As it is very difficult to observe high-field level crossings in a cascade process, the detection of the fluorescent light has to be made directly following excitation of the $^2D_{3/2}$ level. Thus we induce σ transitions from one of the $5\,^2P$ levels and detect the light released in the decay down to the other of the two $5\,^2P$ levels. It is not possible to detect the decay to the same ^2P level because of the stray light from the strong laser beam passing through the cell walls. Even the detection of the decay down to the other fine-structure level is not quite problem free as the wavelength difference between the laser light and the detected light is only about 80 Å. The interference filters we used were not narrow enough to suppress the laser light completely. By painting big parts of the cell and the interior of the apparatus black, the stray light could be reduced but still it frequently had the same intensity as the fluorescent light. However, the stray light was not very detrimental to the signal-to-noise ratio as the laser light intensity averaged over all modes was quite stable, whereas the intensity of the mode(s) hitting the atomic transition was fluctuating as discussed above. The detection line as well as all other visible and uv lines were eliminated from the rf-lamp output by a RG 10 color glass filter.

The level diagram for the $^2D_{3/2}$ states in ^{87}Rb has already been shown in Fig. 3. Out of the four $\Delta m = 2$ level crossings only the first three are suitable for detection. In Fig. 5 experimental curves for the 6 and $7\,^2D_{3/2}$ levels are displayed.

In order to obtain accurate values for the hfs coupling constants we made several runs where the magnetic field sweep only covered a small region over the first crossing or over the second and third crossings. The direction of the steady field was also shifted with respect to Earth's field whereas the direction of the sweep field remained the same. By taking averages over complimentary runs the effects of Earth's field, time constants, and uncertainties in the sweep could be virtually eliminated. Before each series of measurements the phase of the lock-in amplifier was carefully adjusted so that for the Hanle signal a completely symmetric curve was obtained. In this way any dispersion-type signal contributions, caused by the geometrical arrangement, could be eliminated. Because of the slight variation of the matrix elements of Eq. (3) over the half-width of a crossing, a very slight admixture of dispersion curve to the Lorentzian-shaped crossing curve is obtained even for a perfect geometrical arrangement. The second and third crossings in both states slightly overlap and we calculate corrections to obtain the undisturbed crossing positions. We obtain for the first three crossings the field values listed in Table I. The quoted errors comprise two standard deviations of the statistical data, a 0.2% magnetic field uncertainty and estimated errors in the overlap corrections as well as the uncertainty due to a small dispersion-type admixture. For the analysis of our LC results we assume the theoretical value $g_J(^2D_{3/2}) = 0.7995$, which should be accurate for the precision we obtain. With three measured crossing positions for each state the a and b factors are overdetermined. However, the consistency of the results is very good and further indicates that our results are not influenced by light shifts or other systematic effects. Our results for the two studied states are

$$\left.\begin{aligned} |a(6\,^2D_{3/2}\ ^{87}\mathrm{Rb})| &= 7.84(5)\ \mathrm{MHz} \\ |b(6\,^2D_{3/2}\ ^{87}\mathrm{Rb})| &= 0.53(6)\ \mathrm{MHz} \end{aligned}\right\} b/a > 0$$

and

$$\left.\begin{aligned} |a(7\,^2D_{3/2}\ ^{87}\mathrm{Rb})| &= 4.53(3)\ \mathrm{MHz} \\ |b(7\,^2D_{3/2}\ ^{87}\mathrm{Rb})| &= 0.26(4)\ \mathrm{MHz} \end{aligned}\right\} b/a > 0\ .$$

TABLE I. Positions of level-crossing signals in $^2D_{3/2}$ states in ^{87}Rb (magnetic fields in gauss). The crossings are identified by the quantum numbers of the participating levels using the symbol $(F, m_F; F', m_F')$.

State	First crossing (2, −2; 1, 0)	Second crossing (3, −2; 2, 0)	Third crossing (3, −3; 2, −1)
$6\,^2D_{3/2}$	9.280 (30)	15.516 (105)	17.712 (105)
$7\,^2D_{3/2}$	5.392 (25)	8.980 (55)	10.179 (70)

The b factors are obtained with an uncertainty of about 15% and represent the first alkali-metal quadrupole coupling constants obtained for non-P states.

^{87}Rb was preferred to the other stable rubidium isotope ^{85}Rb in this investigation because the former isotope has an about three times larger hfs than the latter which means that a better resolution between the level-crossing signals is obtained. For comparison we also made LC measurements on the $6\,^2D_{3/2}$ state of ^{85}Rb. In this case the first crossing is isolated, whereas the second and third crossings overlap into one signal. The structure closely corresponds to the one expected for the coupling constants calculated from the ^{87}Rb results.

B. Measurements on the 8, 9, and 10 $^2D_{3/2}$ levels in ^{133}Cs

The 8, 9, and 10 $^2D_{3/2}$ levels in ^{133}Cs were studied in very much the same way as were the Rb $^2D_{3/2}$ states. The energy level diagram for the $^2D_{3/2}$ states in ^{133}Cs (nuclear spin $I = \frac{7}{2}$) is shown in Fig. 6. The second and third crossings are very close to each other and cannot be expected to be resolved. As the detection line and the laser excitation line are about 200 Å apart, the suppression of the laser light was much simpler than for Rb. In Fig. 7 experimental curves are shown. For ob-

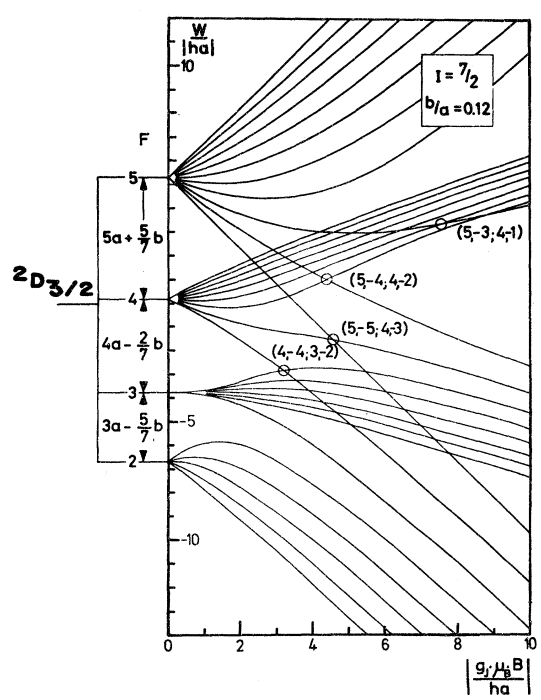

FIG. 6. Energy-level diagram for the hyperfine structure of a $^2D_{3/2}$ state in ^{133}Cs (nuclear spin $I = \frac{7}{2}$). The $\Delta m = 2$ crossings are indicated.

taining a good precision short regions over the signals were covered with the sweep in the averaging process as described above. For the analysis of the data we assume a vanishing b-coupling constant, which is well justified considering the small value of the quadrupole moment of ^{133}Cs($Q = -3$ mb). Even for the $^2P_{3/2}$ states, which should have a higher b/a ratio than the $^2D_{3/2}$ states, and which have a considerably better resolution, the b factor could in no case be determined to a better accuracy than 30% as the quadrupole moment is so small. As the second and third crossings overlap into a structureless curve we replace the two crossings by an "effective" signal, which can be estimated from the theoretical relative signal strengths and half-widths. A detailed analysis was not performed as a high-precision measurement was never attempted since significant quadrupole interaction constants can never be obtained anyway. For the dipole coupling constants we obtain an accuracy of about 2%.

The $^2D_{3/2}$ states can also be studied with ODR in the Paschen-Back region for the hfs. As an example the signal structure obtained for the $9\,^2D_{3/2}$ state in ^{133}Cs is shown in Fig. 8. According to Eq. (6) eight signals of approximately equal intensity are expected around the center of gravity (c.g.) corresponding to $g_J = 0.8$. The structure obtained is unresolved with a total width closely agreeing with the one inferred from the more accurate LC results. From Fig. 8 it is also seen that the Landé factor calculated from Eq. (2) is valid to the accuracy needed in our experiments. Similar experiments were done for the $8\,^2D_{3/2}$ state. At the end of this paragraph we present the results obtained for the studied $^2D_{3/2}$ states in ^{133}Cs:

$$|a(8\,^2D_{3/2}\ ^{133}\mathrm{Cs})| = 3.98(8)\ \mathrm{MHz}\ ,$$

$$|a(9\,^2D_{3/2}\ ^{133}\mathrm{Cs})| = 2.37(3)\ \mathrm{MHz}\ ,$$

$$|a(10\,^2D_{3/2}\ ^{133}\mathrm{Cs})| = 1.52(3)\ \mathrm{MHz}\ .$$

C. Optical double-resonance measurements on the 8, 9, and 10 $^2D_{5/2}$ levels in ^{133}Cs

As the transition between a $^2D_{5/2}$ state and a $^2P_{1/2}$ state is forbidden and the laser transition cannot be used for the detection due to the stray light, a different detection scheme had to be used for the measurements of the highly excited $^2D_{5/2}$ states in ^{133}Cs. No other direct transition from the $^2D_{5/2}$ states falls within the wavelength region for which ordinary photomultiplier tubes can be used. Thus, the fluorescent light released in the second step of a cascading process has to be studied. The highly excited $^2D_{5/2}$ states in Cs decay with a branching ratio of about 15% into the second excited $^2P_{3/2}$ level ($7\,^2P_{3/2}$) and the wavelength for the transition from this state to the ground state is 4555 Å and can be well isolated from both exciting lines. The diagram in the center of Fig. 2 is an example of this two-step fluorescence scheme. Schott BG12 and BG18 color glass filters were useful in further suppressing the background light. As the LC method is not very applicable in

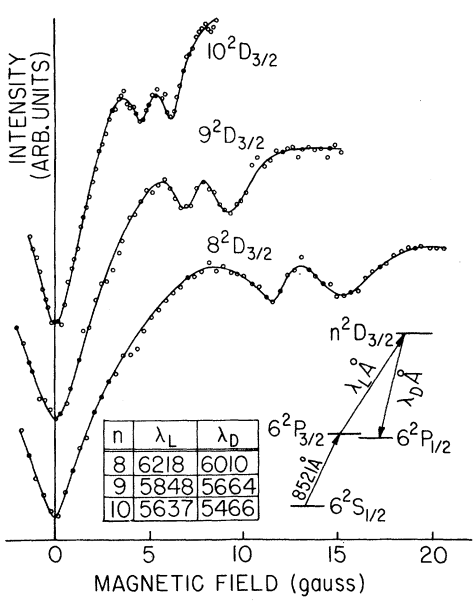

FIG. 7. Experimental curves for LC measurements on the 8, 9, and 10 $^2D_{3/2}$ states in ^{133}Cs. Total sampling time for each curve is about 1 h.

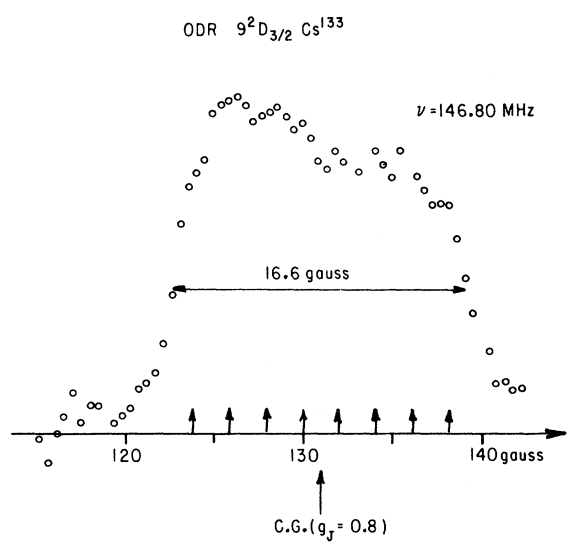

FIG. 8. Optical-double-resonance signal structure obtained in the Paschen-Back region for the hyperfine structure of the $9\,^2D_{3/2}$ state in ^{133}Cs. The theoretical center of gravity for a $^2D_{3/2}$ state is shown as well as the expected signal positions calculated from LC data.

this case for reasons already discussed we used the ODR technique. Various polarization schemes were used in these measurements. In early test runs we used circularly polarized light for the first excitation step and analyzed the degree of circular polarization of the fluorescent light. The laser light was incident on the cell at right angles to the magnetic field and either π or σ excitation was used. Thus the fluorescent light obtains a circular polarization only because of the orientation produced in the intermediate P state ($6\,^2P_{3/2}$). With this arrangement it was very simple to study the multiple-scattering process occurring at higher temperature. Thus it is observed that as the fluorescent light intensity increases with rising vapor pressure the polarization strongly declines due to the isotropic nature of the multiple scattering. Thus although ODR signals can be observed as a decrease in the polarization no improvement in the signal-to-noise ratio is obtained using the multiple-scattering process. Instead it is more suitable to induce the wanted polarization in the second excitation step. Circularly polarized or more conveniently π or σ laser light of linear polarization can be used. The rf fed to the 147-MHz cavity was 100% amplitude modulated for lock-in detection. We detected the intensity of the σ light (σ^+ and σ^-) scattered in the direction of the magnetic field. It was observed, that π excitation resulted in a much stronger resonance signal than did σ excitation. The transfer of rf signals through a branch state can be calculated using Eq. (4). The process was theoretically studied by Gupta, Happer, Lam, and Svanberg.[6]

The 8, 9, and $10\,^2D_{5/2}$ levels in ^{133}Cs all turn out to have a very small hfs. In the Paschen-Back region an unresolved signal structure is observed. Experimental curves are shown in Fig. 9. As in the $^2D_{3/2}$ states, eight signals contribute, corresponding to the different values of m_I. The signals should be symmetrically distributed around the center of gravity corresponding to the g_J factor for the state. The expected position according to Eq. (2) is indicated in the figure and obviously the observed positions vindicate the use of this equation. At the left of each curve the half-width of an individual signal component as calculated from the lifetime predicted by the Coulomb-approximation calculation is shown. The spacing between the signal components is in frequency units equal to the magnetic dipole coupling constant a. The intensity of the signal components should be very closely equal as the used fields decouple the $^2D_{5/2}$ state completely and the $7\,^2P_{3/2}$ state to a very high extent. From Fig. 9 it is evident that a has a nonzero value for all states. In order to obtain information about the hfs we made measuring series in which we extrapolated the signal structure half-width to zero rf power. This is very important as the signal contributions broaden according to Eq. (7). We also investigated that we did not have collisional broadening. We found for the extrapolated half-widths the values 4.5(4), 2.7(4), and 2.3(4) G for the 8, 9, and $10\,^2D_{5/2}$ levels, respectively.

In order to relate the experimental half-widths to the hfs we calculated on a computer the width of the total signal structure as a function of the a factor. In Fig. 10 the result is shown for the $9\,^2D_{5/2}$ state. Three different lifetime values were chosen, of which the intermediate one (183 nsec) is the prediction of our theoretical calculation. The experimental half-width is also indicated and for the a factor an absolute value close to 0.5 MHz is inferred. The 8 and $10\,^2D_{5/2}$ states were treated in the same way. With a conservative estimation of error, also allowing for possible systematic errors, we obtain the following results:

$$|a(8\,^2D_{5/2}\ ^{133}\mathrm{Cs})| = 0.9(4)\ \mathrm{MHz}\ ,$$

$$|a(9\,^2D_{5/2}\ ^{133}\mathrm{Cs})| = 0.5(2)\ \mathrm{MHz}\ ,$$

$$|a(10\,^2D_{5/2}\ ^{133}\mathrm{Cs})| = 0.4(2)\ \mathrm{MHz}\ .$$

In these experiments resonances in the $7\,^2P_{3/2}$ state should also be obtained, as the oberved light would be depolarized by population equalization between pairs of sublevels also in the interme-

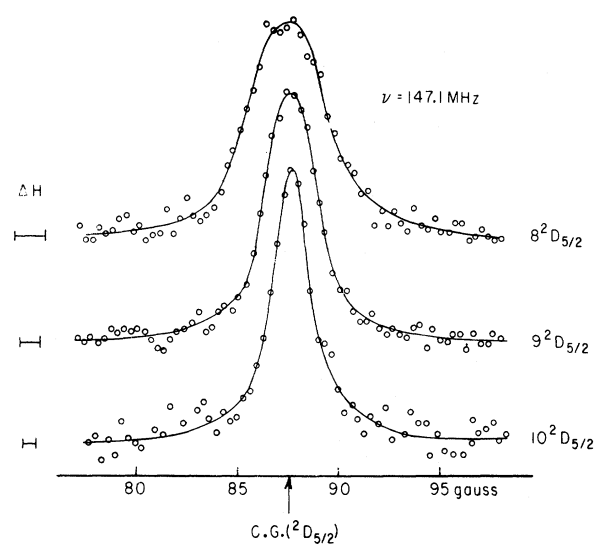

FIG. 9. Optical-double-resonance signals for the 8, 9, and $10\,^2D_{5/2}$ states in ^{133}Cs. The theoretical center of gravity for a $^2D_{5/2}$ state is indicated. To the left of each curve the theoretical width for each of the eight closely spaced signal contributions, making up the signal structure, is shown.

diate state.[6] However, as the hfs is much larger for this state ($a = 16.61$ MHz) the hfs is not completely decoupled and a large number of resonances correspondingly weak are possible. Further, this state has a shorter lifetime ($\tau = 131$ nsec) which further decreases the signal strengths. Consequently, compared to the $^2D_{5/2}$ signal the $^2P_{3/2}$ resonances were very weak and were not observed in our experiments.

D. Optical double-resonance measurements on the 6 and 7 $^2D_{5/2}$ levels in ^{87}Rb

The 6 and 7 $^2D_{5/2}$ in ^{87}Rb were studied with ODR in very much the same way as the $^2D_{5/2}$ states in ^{133}Cs. The investigated rubidium states have a branching ratio into the second excited $^2P_{3/2}$ state ($6\,^2P_{3/2}$) of about 7%. In the Paschen-Back region for the hfs four signals are obtained. In Fig. 11 experimental curves and level diagrams, showing the two-step excitation and the two-step decay are displayed. A more favorable ratio between the hfs and the radiative widths is obtained for Rb. Thus the four resonances in the $6\,^2D_{5/2}$ state give rise to a partly resolved structure. As in the case of Cs we do not observe resonances in the $6\,^2P_{3/2}$ state of ^{87}Rb. From an analysis of curves like the ones in Fig. 11 we obtain the following absolute values for the dipole interaction constant a:

$$|a(6\,^2D_{5/2}\ ^{87}\mathrm{Rb})| = 3.6(7)\ \mathrm{MHz}\ ,$$

$$|a(7\,^2D_{5/2}\ ^{87}\mathrm{Rb})| = 2.2(5)\ \mathrm{MHz}\ .$$

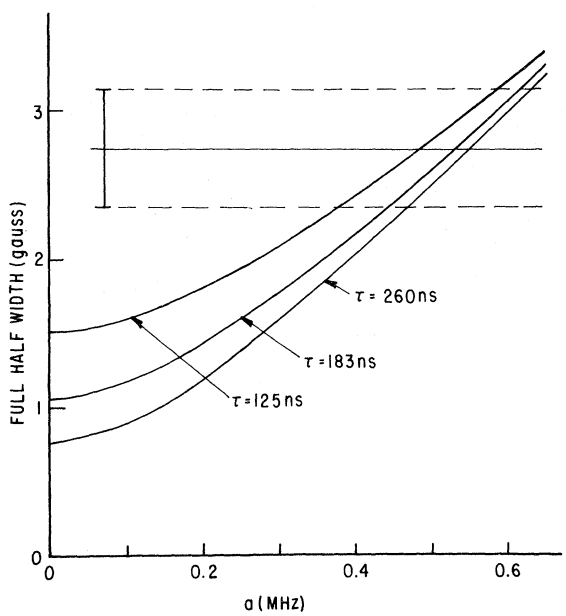

FIG. 10. Diagram for evaluating the dipole interaction constant a for the $9\,^2D_{5/2}$ state is ^{133}Cs. Theoretical curves for the half-width of the ODR signal structure is shown as a function of a for different lifetime values τ. The experimentally found half-width is compatible with an a factor of absolute value close to 0.5 MHz.

VI. ANALYSIS

As already mentioned the signs of the dipole interaction constants, measured to absolute value in this work, have been determined in subsequent Stark-effect measurements.[20] All $^2D_{3/2}$ states were found to have positive a factors, whereas the $^2D_{5/2}$ states all have a negative a factor. The negative sign, which has been found earlier for lower $^2D_{5/2}$ states, is a striking feature, illuminating the strong perturbations present for the D states. In Table II the experimental dipole interaction constants for ^2D states in ^{87}Rb and ^{133}Cs are collected. Data for lower-lying states previously investigated have been included for completeness. The $^2D_{5/2}$ states studied in this work have also been investigated by level-crossing spectroscopy on an atomic beam.[20] The a values for the $^2D_{5/2}$ states given in Table II are mean values from the ODR and LC measurements.

In a general treatment of the magnetic-dipole interaction the following effective Hamiltonian is obtained[22]:

$$H_{\mathrm{dip}} = 2\mu_B^2 g_I' [\vec{l}\langle r^{-3}\rangle_l - \sqrt{10}\ (\vec{s}\cdot\overleftrightarrow{C}^{(2)})^{(1)} \times \langle r^{-3}\rangle_{\mathrm{sd}} + \vec{s}\langle r^{-3}\rangle_s]\cdot\vec{I}\ . \tag{8}$$

Here $\vec{l}$, $(\vec{s}\cdot\overleftrightarrow{C}^{(2)})^{(1)}$, and $\vec{s}$ are the orbital, spin-dipole, and Fermi contact operators, respectively. Using this operator for ^2D states one can show that the resulting magnetic dipole interaction constants $a(^2D_{3/2})$ and $a(^2D_{5/2})$ can be expressed as

$$a(^2D_{3/2}) = \frac{2\mu_B^2 g_I'}{h}\left(\tfrac{6}{5}\langle r^{-3}\rangle_l + \tfrac{2}{5}\langle r^{-3}\rangle_{\mathrm{sd}} - \tfrac{1}{5}\langle r^{-3}\rangle_s\right), \tag{9a}$$

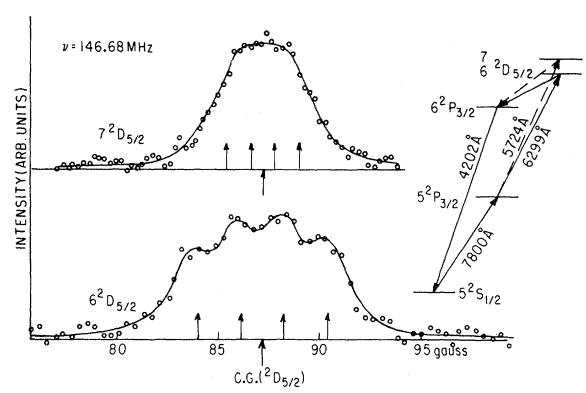

FIG. 11. Optical-double-resonance signal structures for the 6 and $7\,^2D_{5/2}$ states in ^{87}Rb. The theoretical center of gravity as well as the positions of the four signals making up the observed signal structure are shown.

$$a(^2D_{5/2}) = \frac{2\mu_B^2 g_I'}{h}\left(\tfrac{4}{5}\langle r^{-3}\rangle_l - \tfrac{4}{35}\langle r^{-3}\rangle_{sd} + \tfrac{1}{5}\langle r^{-3}\rangle_s\right). \tag{9b}$$

The parameters $\langle r^{-3}\rangle$ can be determined if $a(^2D_{3/2})$ and $a(^2D_{5/2})$ are measured, and if one more independent relationship between the parameters $\langle r^{-3}\rangle$ is known from experiment. This can be found by making measurements in magnetic fields strong enough to decouple the spin and angular momenta of the electron. Actually, such high-field measurements have been performed for the $4\,^2D$ state in rubidium by Liao *et al.*[23] It was found that $\langle r^{-3}\rangle_l$ and $\langle r^{-3}\rangle_{sd}$ have opposite signs and the parameter $\langle r^{-3}\rangle_s$ is very large. In his recent perturbative calculations for ^2D states in rubidium, Lindgren[24] obtains similar results also for the higher members of the D sequence. High-field experiments for these states are in preparation in Göteborg. For cesium no experimental or theoretical results for the individual $\langle r^{-3}\rangle$ parameters are available.

The quadrupole interaction constant b is related to the nuclear quadrupole moment Q by the equation

$$b = \frac{e^2}{h}\,\frac{2j-1}{2j+2}\,Q\langle r^{-3}\rangle_q\ , \tag{10}$$

TABLE II. Experimental magnetic dipole interaction constants for ^2D levels in ^{87}Rb and ^{133}Cs.

Element	State	a_{expt} (MHz)	b_{expt} (MHz)
^{87}Rb	$4\,^2D_{3/2}$	25.1 (9) [a]	
	$4\,^2D_{5/2}$	−16.9 (6) [a]	
	$5\,^2D_{3/2}$	14.43 (12) [b]	
	$5\,^2D_{5/2}$	− 7.44 (6) [b]	
	$6\,^2D_{3/2}$	7.84 (5) [c]	0.53 (6) [c]
	$6\,^2D_{5/2}$	− 3.4 (5) [c]	
	$7\,^2D_{3/2}$	4.53 (3) [c]	0.26 (4) [c]
	$7\,^2D_{5/2}$	− 2.0 (3) [c]	
^{133}Cs	$6\,^2D_{3/2}$	16.38 (5) [d]	
	$6\,^2D_{5/2}$	− 3.0 (1.0) [d]	
	$8\,^2D_{3/2}$	3.98 (18) [c]	
	$8\,^2D_{5/2}$	− 0.85 (20) [c]	
	$9\,^2D_{3/2}$	2.37 (3) [c]	
	$9\,^2D_{5/2}$	− 0.45 (10) [c]	
	$10\,^2D_{3/2}$	1.52 (3) [c]	
	$10\,^2D_{5/2}$	− 0.35 (10) [c]	

[a] Reference 23.
[b] Reference 5.
[c] This work and Ref. 20.
[d] C. Tai, thesis (Columbia University, 1974) (unpublished).

where $\langle r^{-3}\rangle_q$ is the radial parameter for the quadrupole interaction. For P states $\langle r^{-3}\rangle_q$ can be obtained from $\langle r^{-3}\rangle_l$ using the correction factors calculated by Sternheimer.[25] Sternheimer has also calculated corresponding correction factors for D states.[26] These factors are, however, hard to apply for the strongly perturbed D states in rubidium as discussed by Lindgren.[24]

It seems that the hyperfine structure of the D states of the rubidium can be calculated to some reliability only by elaborate *ab initio* calculations, e.g., of the many-body perturbation type. Some first results have been obtained by Lindgren,[24] who lists the $\langle r^{-3}\rangle$ parameters for the 4–$8\,^2D$ states with the effect of second-order polarization included. In Table III the experimental a and b factors for the 6 and $7\,^2D$ states of ^{87}Rb are listed together with a factors, calculated by Eqs. (9a) and (9b) and using Lindgren's $\langle r^{-3}\rangle$ parameters. The table also contains the values of the quadrupole moment deduced from the experimental b factors using Eq. (10). Q_a are the calculated values using Lindgren's $\langle r^{-3}\rangle_q$ parameter, whereas Q_b are values obtained in a semiempirical procedure, utilizing the experimental magnetic hfs to correct the $\langle r^{-3}\rangle_q$ parameter.[24] The calculated Q values are to be compared with $Q = 0.13$ b, the value obtained from the comparatively undisturbed $^2P_{3/2}$ states of ^{87}Rb. Although the theoretical a factors are a factor of about 2 too small, the correct signs and the correct ratios are obtained. A reasonable value for the quadrupole moment is also obtained. Clearly, the calculations must be performed to higher order including also correlation effects before a more detailed agreement can be expected. However, the results obtained so far seem to encourage further work, theoretically as well as experimentally.

TABLE III. Comparison between experimental values for ^{87}Rb and values calculated using Lindgren's parameters (Ref. 24). Calculated values for the quadrupole moment are from D-state data.

State	a_{theor} (MHz)	a_{expt} (MHz)	b_{expt} (MHz)	Q_a (b)	Q_b (b)
$6\,^2D_{3/2}$	3.26	7.84 (5)	0.53 (6)	0.21	0.17
$6\,^2D_{5/2}$	−1.52	−3.4 (5)			
$7\,^2D_{3/2}$	2.00	4.53 (3)	0.26 (4)	0.18	0.15
$7\,^2D_{5/2}$	−0.88	−2.0 (3)			
				$Q_{\text{"correct"}} = 0.13$	

ACKNOWLEDGMENTS

The authors want to thank Professor W. Happer for most valuable discussions and continuing support. We are also very grateful to Dr. R. Gupta for advice and assistance. Further, thanks are due to J. Farley for assistance. One of the authors (S.S.) wishes to thank the staff of the Columbia Radiation Laboratory for the warm hospitality extended to him during a year's stay at Columbia University.

---

*Work supported in part by the Joint Services Electronics Program (U.S. Army, U.S. Navy, U.S. Air Force) under Contract No. DAAB07-69-C-0383, and in part by the Air Force Office of Scientific Research under Grant No. AFOSR 72-2180.

†Permanent address: Department of Physics, Chalmers University of Technology, Fack, S-402 20 Göteborg, Sweden.

‡Supported in part by the Swedish Natural Science Research Council.

[1]C. E. Moore, *Atomic Energy Levels*, Natl. Bur. Stds. Circ. No. 467 (U.S. GPO, Washington, D.C., 1958).

[2]H. Kopfermann, *Nuclear Moments* (Academic, New York, 1968).

[3]Y. Archambault, J. P. Descourbes, M. Priou, A. Omont, and J. C. Pébay-Peyroula, J. Phys. Radium 21, 677 (1960).

[4]S. Chang, R. Gupta, and W. Happer, Phys. Rev. Lett. 27, 1036 (1971).

[5]R. Gupta, S. Chang, C. Tai, and W. Happer, Phys. Rev. Lett. 29, 695 (1972).

[6]R. Gupta, S. Chang, and W. Happer, Phys. Rev. A 6, 529 (1972); L. K. Lam, R. Gupta, and W. Happer, Bull. Am. Phys. Soc. 18, 121 (1972); R. Gupta, W. Happer, L. K. Lam, and S. Svanberg, Phys. Rev. A 8, 2792 (1973); K. H. Liao, R. Gupta, and W. Happer, Phys. Rev. A 8, 2811 (1973).

[7]S. Svanberg, P. Tsekeris, and W. Happer, Bull. Am. Phys. Soc. 18, 611 (1973).

[8]S. Svanberg, P. Tsekeris, and W. Happer, Phys. Rev. Lett. 30, 817 (1973); S. Svanberg, in *International Conference in Laser Spectroscopy, Vail, Colorado, 1973*, edited by R. G. Brewer and A. Mooradian (Plenum, New York, 1974).

[9]B. P. Kibble and S. Pancharatnam, Proc. Phys. Soc. Lond. 86, 1351 (1965).

[10]W. Hanle and R. Pepperl, in *Physics of the One- and Two-Electron Systems*, edited by Bopp and Kleinpoppen (North-Holland, Amsterdam, 1968).

[11]R. L. Smith and T. G. Eck, Phys. Rev. A 2, 2179 (1970).

[12]D. J. Bradley, G. M. Gale, and R. D. Smith, J. Phys. B 3, L11 (1970).

[13]D. J. Bradley, in *International Conference in Laser Spectroscopy, Vail, Colorado, 1973*, edited by R. G. Brewer and A. Mooradian (Plenum, New York, 1974); D. J. Bradley, P. Ewart, J. V. Nicholas, J. R. Shaw, and D. G. Thompson, Phys. Rev. Lett. 31, 263 (1973).

[14]W. Gornik, D. Kaiser, and W. Lange, J. Luther, H. H. Radloff, and H. H. Schulz, Appl. Phys. 1, 285 (1973).

[15]See, e.g., G. zu Putlitz, in *Proceedings of the International Conference on Atomic Physics, New York*, edited by B. Bederson, B. W. Cohen and F. M. J. Pichanick (Plenum, New York, 1969); W. Fischer, Fortschr. Phys. 18, 89 (1970); D. Feiertag and G. zu Putlitz, Z. Phys. 261, 1 (1973); S. Svanberg, Phys. Scr. 4, 275 (1971); B. Belin and S. Svanberg, Phys. Scr. 5, 209 (1972).

[16]G. Breit, Rev. Mod. Phys. 5, 91 (1933); P. A. Franken, Phys. Rev. 121, 508 (1961).

[17]H. H. Stroke, G. Fulop, S. Klepper, and O. Redi, Phys. Rev. Lett. 21, 61 (1968).

[18]A. Ellet and N. P. Heydenburg, Phys. Rev. 46, 583 (1934); N. P. Heydenburg, *ibid.* 46, 802 (1934).

[19]See, e.g., P. Zimmermann, Z. Phys. 226, 415 (1969).

[20]W. Hogervorst and S. Svanberg, Z. Phys. (to be published).

[21]D. P. Bates and A. Damgaard, Philos. Trans. R. Soc. Lond. 242, 101 (1949); O. S. Heavens, J. Opt. Soc. Amer. 51, 1058 (1961).

[22]L. Armstrong, Jr., *Theory of the Hyperfine Structure of Free Atoms* (Wiley, New York, 1971); P. G. H. Sandars and J. Beck, Proc. R. Soc. Lond. A 289, 97 (1965); I. Lindgren and A. Rosén, Case Studies in At. Phys. 4, 93 (1974) and 4, 197 (1974).

[23]K. H. Liao, L. K. Lam, R. Gupta, and W. Happer, Phys. Rev. Lett. 32, 1340 (1974).

[24]I. Lindgren, *Atomic Physics 4, Proceedings of the Fourth International Conference on Atomic Physics, Heidelberg 1974* (Plenum, New York, to be published); I. Lindgren (private communication).

[25]See, e.g., R. M. Sternheimer and R. F. Peierls, Phys. Rev. A 3, 837 (1971).

[26]R. M. Sternheimer, Phys. Rev. A 9, 1783 (1974).